# Direct imaging of localized surface plasmon polaritons

**Sinan Balci,* Ertugrul Karademir, Coskun Kocabas, and Atilla Aydinli**

*Department of Physics, Advanced Research Laboratories and Turk Telekom Laboratory, Bilkent University, 06800 Ankara, Turkey*
**Corresponding author: balci@fen.bilkent.edu.tr*

Received June 27, 2011; revised August 4, 2011; accepted August 4, 2011;
posted August 5, 2011 (Doc. ID 150030); published August 26, 2011

In this Letter, we report on dark field imaging of localized surface plasmon polaritons (SPPs) in plasmonic waveguiding bands formed by plasmonic coupled cavities. We image the light scattered from SPPs in the plasmonic cavities excited by a tunable light source. Tuning the excitation wavelength, we measure the localization and dispersion of the plasmonic cavity mode. Dark field imaging has been achieved in the Kretschmann configuration using a supercontinuum white-light laser equipped with an acoustooptic tunable filter. Polarization dependent spectroscopic reflection and dark field imaging measurements are correlated and found to be in agreement with finite-difference time-domain calculations. 

*OCIS codes:* 240.6680, 250.5403, 050.2770.

Imaging of surface plasmon polaritons (SPPs), coupled electromagnetic field-charge density oscillation at a metal-dielectric interface, has attracted great interest in recent years due to the possibility of obtaining subwavelength plasmonic optics [1–10]. Plasmonic imaging with subwavelength resolution is another interesting application of plasmonics. The SPP waves around the metallic nanostructures can be imaged, for example using a scanning near-field optical microscope (SNOM) or a photon scanning tunneling microscope (PSTM) by raster scanning the sharpened fiber tip in the near-field over a metallic surface to obtain an optical image with subwavelength resolution [2–5]. In this way, plasmonic properties of individual metallic nanoparticles have been measured different from the nanoparticle ensemble. Using PSTM, Dawson *et al.* have shown the first direct imaging of propagating SPP waves and directly calculated the propagation length of SPPs [2]. PSTM imaging of sampled Bragg mirrors containing coupled SPP cavities has been also achieved [3]. However, SNOM or PSTM imaging entail significant experimental effort, and the interaction between the sample and the tip may affect the experimental results. An alternative way of imaging SPPs is using total internal reflection or dark field microscopy [6–10]. Different from conventional bright field optical microscopy, dark field imaging involves suppression of specular reflection and detection of the scattered light from the sample. Performing dark field imaging of nanowires and nanoparticles, Sonnichsen *et al.* have determined the plasmon resonance of individual gold nanoparticles [8]. Moreover, using dark field imaging of SPP waves, it has been shown that a drastic reduction of the plasmon dephasing rate in metallic nanowires occurs when compared with small metallic nanoparticles [8]. In contrast with previous studies, here we use dark field microscopy to directly image localized SPPs in plasmonic coupled cavities [11–17]. We correlate spectroscopic reflection and dark field imaging measurements to shed light on the spatial distribution of SPPs in the cavity region. By tuning the coupling coefficient between the cavities we control the group velocity and dispersion of SPPs. By directly imaging SPP waves in the cavity region, we show that as the coupling coefficient between the cavities goes to zero, localization of SPPs increases.

Fabrication of plasmonic cavities on moiré surfaces has been achieved using a holographic technique called interference lithography, details of which we reported earlier [11–14]. Figures 1(a) and 1(b) show scanning electron microscope (SEM) and atomic force microscope (AFM) images of one-dimensional SPP cavities, respectively. The micrograph in Fig. 1(a) shows an array of coupled cavities, whereas the one in Fig. 1(b) shows a single cavity. It is obvious that the amplitude of the moiré surface approaches zero in the vicinity of the nodes where the cavity is located. In reflection measurements, the depth of the grating has to be properly adjusted to observe the dispersion of SPPs since the dispersion of SPPs strongly depends on the grating groove depth [13]. In order to tune the groove depth, exposure time of the photopolymer was varied. A thin layer of Ag film (~35 nm) was evaporated on the patterned surface to support the propagation of SPPs. The Kretschmann configuration was established by attaching the glass sample onto a prism using index matching fluid. Reflectivity measurements were performed by varying the incidence angle and monitoring the reflected light as a function of wavelength using a spectroscopic ellipsometer [11–14]. Dark field plasmon microscopy (DFPM) imaging was performed using a supercontinuum white-light laser as an excitation source (Fig. 2) [6–10]. The supercontinuum light source is a spatially coherent broad band source (500–1800 nm) with very high spectral power density (2.5 $\mu$W at 615 nm during imaging). An acousto-optic tunable filter (AOTF) can select the desired wavelength from the broad range of available wavelengths. The excitation light is introduced into the sample at an incidence angle

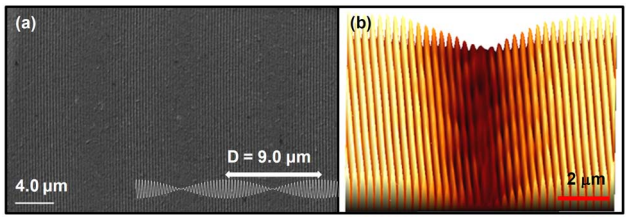


Fig. 1. (Color online) (a) SEM image of 9.0 $\mu$m long plasmonic coupled cavities. Three coupled cavities can be observed in the image. (b) AFM image of a single cavity. The cavity is located where the amplitude of the moiré surface approaches zero.

 

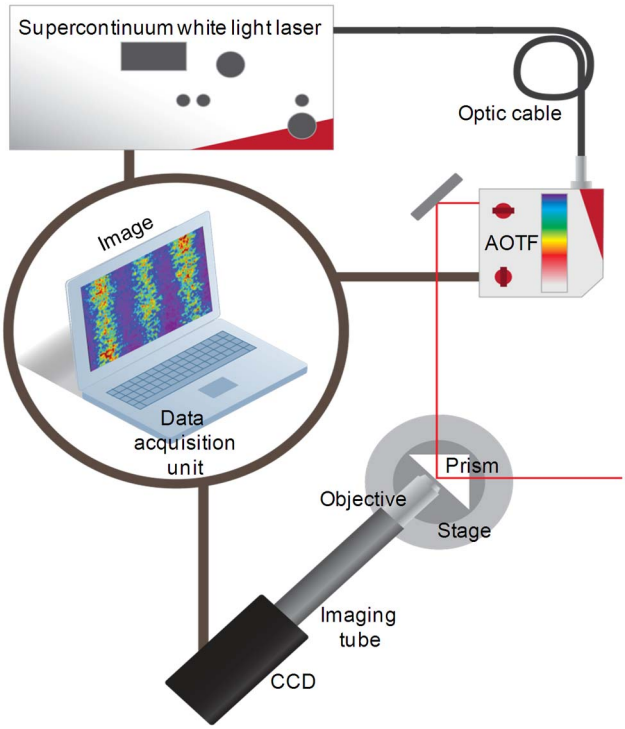


Fig. 2. (Color online) Detailed schematic representation of the experimental apparatus used to image SPP waves on moiré surfaces. A supercontinuum white-light laser with attached AOTF has been used as an excitation laser. Cavity mode can be selectively illuminated to observe the spatial distribution of SPP waves in the cavity region. The scattered SPP waves from the cavity region are collected by an objective and are directly imaged using a digital CCD camera.

larger than the critical angle, which prevents the exciting light from entering the detection optics.

Scanning along the vertical axis of the dispersion curve, SPP cavity modes are excited when the incident light is in resonance with the mode. The SPP field confined to the cavity region is scattered to the far field by the rough metal surface of a few nanometers [17,18]. The scattered SPPs from the cavity mode can be imaged using DFPM giving spatial distribution of SPP waves in the cavity region. A 40× objective is used to collect the light scattered to the far field. The bandwidth of the excitation light is less than 5 nm, while the incident power is 2.5 $\mu$W (at 615 nm) before it hits the sample.

Figure 3(a) shows a dispersion curve of 15.0 $\mu$m long SPP cavities. The curve indicates a bandgap where a band of wavelengths are forbidden and a well localized cavity mode of ~615 nm inside the bandgap region. We have previously shown that this cavity mode band can be modeled using a tight binding approach as it was also applied to coupled resonator optical waveguides [12,13]. Dispersion of the cavity mode can be described as

$$\omega(k) = \Omega[1 + \kappa \cos(kD)], \tag{1}$$

where $\Omega$, $\kappa$, and $D$ are the resonance frequency of the individual cavity, cavity-to-cavity coupling coefficient, and the size of the cavity, respectively. It should be noted that $\kappa$ is a function of both the proximity of the cavities as well as confinement characteristics of each cavity, namely, of the groove depth. The group velocity of the SPP waves can be found as

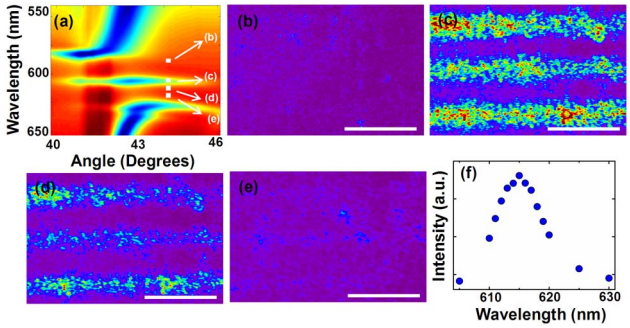


Fig. 3. (Color online) (a) Experimental dispersion curve of 15.0 $\mu$m long SPP cavities showing a bandgap and a cavity state. DFPM image of 15.0 $\mu$m long three SPP cavities imaged with the laser wavelengths of (b) 580 nm, (c) 615 nm, (d) 620 nm, and (e) 630 nm. The white colored bar indicates a 15.0 $\mu$m long distance. (h) Calculated intensity of the cavity mode from DFPM images. The intensity of the scattered light maximizes at ~615 nm, which is the cavity mode in (a).

$$v_g(k) = d\omega(k)/dk = -\Omega D\kappa \sin(kD), \tag{2}$$

which can be quite small when the cavities are weakly coupled. The slope of the dispersion curve gives the group velocity of the cavity modes [Fig. 3(a)]. It is clear that the group velocity and the dispersion of SPPs are a function of the coupling coefficient of the cavities. Thus, in order to significantly slow SPPs, the coupling coefficient has to be very small. The dispersion curve in Fig. 3(a) clearly reveals that SPPs are almost completely stopped at the plasmonic cavity mode since the slope of the cavity mode is almost zero. The same sample has been imaged using DFPM by varying the incident laser wavelength, as pointed out in Fig. 3(a). Figures 3(b)–3(e) show DFPM images of three cavities with varying incident laser wavelengths. The scattered light from the SPPs are collected in the far field by a CCD camera, and images are formed with exposure time of 1 s. It should be noted that SPPs remain nonradiating as long as they propagate on a surface which is translationally invariant in the propagation direction where SPPs decay only by ohmic losses in the metal [18,19]. However, surface roughness will cause scattering of SPP waves due to the breakdown of translational invariance and, therefore, scattered SPPs can be detected in the near or far fields using a suitable optical detection system [18,19]. When SPPs scatter from the surface, the SPP wave can transfer part of its momentum to the defect and decay into a photon. Each line in Figs. 3(b)–3(d) represents the light scattered from one cavity. Figure 3(f) shows intensity of the scattered SPPs as a function of the laser wavelength. The DFPM images with high contrast show that spatial localization of cavity mode occurs at 615 nm, which is the cavity mode in the dispersion curve [Fig. 3(a)]. It is noteworthy to mention here that we have also performed DFPM imaging experiments with cavity sizes smaller than 15.0 $\mu$m and observed substantially decreased contrasts in the images, which is due to the fact that localization of SPPs decreases when the cavity size decreases for a fixed grating groove depth.

Furthermore, the coupling coefficient between the 15.0 $\mu$m long cavities was varied by tuning the grating groove depth resulting in the modification of group

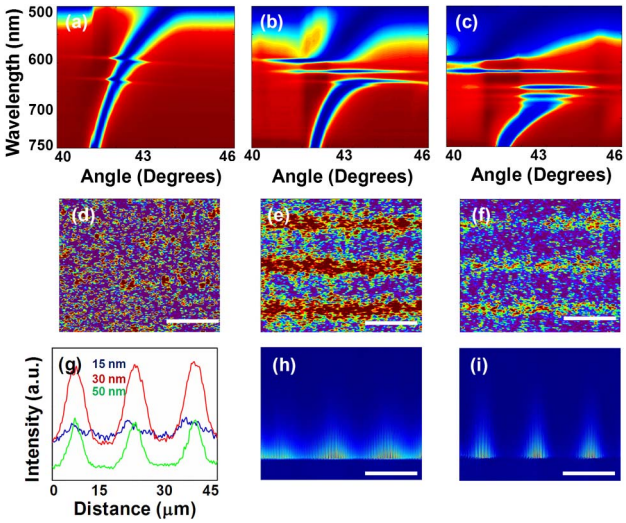


Fig. 4. (Color online) Experimental dispersion curves showing the bandgap and cavity state for 15.0 $\mu$m long cavities with grating groove depths of (a) 15 nm, (b) 30 nm, and (c) 50 nm. DFPM images of three cavities with grating groove depths of (d) 15 nm, (e) 30 nm, and (f) 50 nm. DFPM imaging is performed at an incidence angle of ~42.5°, and the wavelength of the incident light is ~615 nm. (g) Line profiles perpendicular to the long axis of the cavities indicate the intensity of the scattered SPP waves from the cavity region. FDTD calculated two-dimensional electric field distribution at the cavity wavelength for 15.0 $\mu$m long three plasmonic cavities with grating groove depth of (h) 15 nm, and (i) 50 nm. As the depth of the grating groove increases, localization of SPPs in the cavities increases as well. The white colored bars indicate a 15.0 $\mu$m long distance. The vertical length of the images in (h) and (i) is ~2 $\mu$m long.

velocity and dispersion of SPPs. Figures 4(a)–4(c) show dispersion curves of cavities with the groove depths of 15, 30, and 50 nm, respectively. High-order Bragg reflections appear as the grating groove depth increases [3].

It is obvious that the group velocity of SPPs can be significantly decreased (~0 c) (c being the speed of light in vacuum) when the groove depth increases since the slope of the cavity mode in the dispersion curve decreases as the depth increases. The experimental dispersion curves shown in Figs. 4(a)–4(c) have been reproduced using FDTD calculations for the depths of 15, 30, and 50 nm. Figures 4(d)–4(f) indicate DFPM images of 15.0 $\mu$m long cavities at 615 nm cavity resonance wavelength with grating groove depths of 15, 30, and 50 nm, respectively. Figure 4(g), demonstrating the line scans from the DFPM images perpendicular to the long axis of the cavities, indicates that spatial FWHM of the intensity peaks in Fig. 4(g) decreases with the increase in grating depth. FDTD calculated field distribution around the cavity region is shown for grating groove depth of 15 nm in Fig. 4(h), and 50 nm in Fig. 4(i). The DFPM images and the corresponding line scans reveal that as the depth of the grating groove increases, the confinement of SPPs in the cavity region increases, showing the transition from collective modes (delocalized) to isolated modes (localized). Both the reflection measurements and DFPM imaging indicated spatial localization of SPPs in cavities in agreement with the FDTD calculations.

In conclusion, we have shown direct imaging of localized SPP waves in plasmonic cavities by DFPM. Tuning the excitation wavelength, we measure the spatial distribution and dispersion of SPP waves in the cavities. When the size of the SPP cavities is very large, coupling coefficient between the cavities approaches zero and hence each cavity behaves like an isolated cavity separated from the ensemble. Transition from collective cavity modes to isolated cavity modes, observable using DFPM, can be achieved by tuning the Bragg grating groove depth. Spectroscopic reflection and DFPM measurements are correlated and found to be in agreement with FDTD calculations. Small group velocities (~0 c) and localized behavior of SPPs on coupled plasmonic cavities are promising for spectroscopic and nanophotonics applications.

This work has been supported by grants from the Scientific and Technological Research Council of Turkey (110T790, 110T589) and Unam-Regpot (203953). S. Balci acknowledges TUBITAK.

**References**

1. H. Raether, *Surface Plasmons* (Springer, 1986).
2. P. Dawson, F. de Fornel, and J.-P. Goudonnet, Phys. Rev. Lett. **72**, 2927 (1994).
3. J.-C. Weeber, A. Bouhelier, G. C. des Francs, S. Massenot, J. Grandidier, L. Markey, and A. Dereux, Phys. Rev. B **76**, 113405 (2007).
4. D. W. Pohl, W. Denk, and M. Lanz, Appl. Phys. Lett. **44**, 651 (1984).
5. T. Klar, M. Perner, S. Grosse, G. von Plessen, W. Spirkl, and J. Feldmann, Phys. Rev. Lett. **80**, 4249 (1998).
6. M. Hu, C. Novo, A. Funston, H. Wang, H. Staleva, S. Zou, P. Mulvaney, Y. Xia, and G. V. Hartland, J. Mater. Chem. **18**, 1949 (2008).
7. L. Helden, E. Eremina, N. Riefler, C. Hertlein, C. Bechinger, Y. Eremin, and T. Wriedt, Appl. Opt. **45**, 7299 (2006).
8. C. Sonnichsen, S. Geier, N. E. Hecker, G. von Plessen, J. Feldmann, H. Ditlbacher, B. Lamprecht, J. R. Krenn, F. R. Aussenegg, V. Z. H. Chan, J. P. Spatz, and M. Moller, Appl. Phys. Lett. **77**, 2949 (2000).
9. C. Sonnichsen, T. Franzl, T. Wilk, G. von Plessen, J. Feldmann, O. Wilson, and P. Mulvaney, Phys. Rev. Lett. **88**, 077402 (2002).
10. H. Ditlbacher, A. Hohenau, D. Wagner, U. Kreibig, M. Rogers, F. Hofer, F. R. Aussenegg, and J. R. Krenn, Phys. Rev. Lett. **95**, 257403 (2005).
11. S. Balci, A. Kocabas, C. Kocabas, and A. Aydinli, Appl. Phys. Lett. **98**, 031101 (2011).
12. A. Kocabas, S. S. Senlik, and A. Aydinli, Phys. Rev. Lett. **102**, 063901 (2009).
13. S. Balci, A. Kocabas, C. Kocabas, and A. Aydinli, Appl. Phys. Lett. **97**, 131103 (2010).
14. S. Balci, C. Kocabas, and A. Aydinli, Opt. Lett. **36**, 2770 (2011).
15. E. Cubukcu, E. A. Kort, K. B. Crozier, and F. Capasso, Appl. Phys. Lett. **89**, 093120 (2006).
16. Y. Gong and J. Vuckovic, Appl. Phys. Lett. **90**, 033113 (2007).
17. M. Bayindir, B. Temelkuran, and E. Ozbay, Phys. Rev. Lett. **84**, 2140 (2000).
18. I. I. Smolyaninov, D. L. Mazzoni, J. Mait, and C. C. Davis, Phys. Rev. B **56**, 1601 (1997).
19. F. Pincemin, A. A. Maradudin, A. D. Boardman, and J.-J. Greffet, Phys. Rev. B **50**, 15261 (1994).